

## Article

# Deformation Mechanisms of Magnesium Silicate Hydrate Cement with a Shrinkage-Reducing Admixture under Different Curing Conditions

Tingting Zhang , Hao Fu and Junnan Han \*

Faculty of Infrastructure Engineering, Dalian University of Technology, Dalian 116024, China; tingtingzhang@dlut.edu.cn (T.Z.)

\* Correspondence: junnanhan@dlut.edu.cn; Tel.: +86-0411-84707171

**Abstract:** Magnesium silicate hydrate (M-S-H) cement, a type of green building material, has poor volume stability (i.e., large shrinkage deformation), which limits its application. As a new type of admixture, the behavior of a shrinkage-reducing admixture (SRA) in M-S-H cement has not been studied. Therefore, in this research, the effect of SRA on the shrinkage properties of the M-S-H cement system was evaluated. The mechanism of SRA was investigated by surface tension measurement, hydration heat testing, thermogravimetric analysis, and pore structure analysis. Experimental results indicate that SRA can reduce the shrinkage of the M-S-H mortar, and the optimal effect is exerted when the dosage is 3.0%, drying shrinkage decreases by 22.6%, and autogenous shrinkage decreases by 60% on day 28. However, it may also adversely affect strength development. The presence of SRA in M-S-H cement can reduce pore solution surface tension, delay hydration, and maintain relative humidity within the slurry, which can be maintained at 82.0% on day 28. It can also increase pore size and porosity. The inhibitory effect of SRA on the shrinkage of M-S-H mortar is valuable for its future practical applications.

**Keywords:** shrinkage-reducing admixture; magnesium silicate hydrate; drying shrinkage; autogenous shrinkage



**Citation:** Zhang, T.; Fu, H.; Han, J. Deformation Mechanisms of Magnesium Silicate Hydrate Cement with a Shrinkage-Reducing Admixture under Different Curing Conditions. *Minerals* **2023**, *13*, 563. <https://doi.org/10.3390/min13040563>

Academic Editor: Elsabe Kearsley

Received: 6 March 2023

Revised: 11 April 2023

Accepted: 12 April 2023

Published: 17 April 2023



**Copyright:** © 2023 by the authors. Licensee MDPI, Basel, Switzerland. This article is an open access article distributed under the terms and conditions of the Creative Commons Attribution (CC BY) license (<https://creativecommons.org/licenses/by/4.0/>).

## 1. Introduction

In construction, deformation of cement-based materials is a critical factor affecting their safety, durability, and appearance. Stress caused by an excessive change in volume can result in cracks in weak areas, affecting mechanical properties and providing channels for the medium to invade, which can accelerate structural destruction [1]. Magnesium silicate hydrate (M-S-H) cement is a type of green cementitious material [2]. It is lightweight, has low alkalinity, and exhibits excellent mechanical properties. M-S-H cement has a porous structure and a large specific surface area, and its hydration products can form stone and magnesium olivine that can resist high temperatures after calcination. These characteristics endow M-S-H cement with the potential to prepare refractory and thermal insulation materials, seal nuclear waste, and solidify heavy-metal ions [3–5]. Owing to these characteristics, M-S-H cement has drawn interest in the building industry. Although M-S-H cement has numerous advantages, its development is restricted by shortcomings, including high water demand and shrinkage deformation. Innovative solutions need to be implemented. Previous studies have found that the shrinkage of M-S-H mortar is mainly attributed to drying shrinkage and autogenous shrinkage [6]. However, few studies have reported on the control of volume deformation in M-S-H cement. The incorporation of quartz sand into M-S-H cement can improve its volume stability during the drying process and avoid cracking [7]. Li et al. added superabsorbent polymer to M-S-H cement, and the internal curing water stored in the polymer facilitated the hydration process. At the same time, the volume of large pores was increased and the volume of capillary

pores reduced, which effectively reduced the autogenous shrinkage caused by capillary tension [8]. However, studies on the shrinkage of M-S-H mortar remain scarce. Further research on methods by which shrinkage in an M-S-H mortar may be effectively controlled needs to be conducted.

A shrinkage-reducing admixture (SRA) is a cement-based material admixture that can reduce the shrinkage of materials to inhibit cracking [9]. Research indicates that the use of SRA in cement-based materials can effectively reduce shrinkage [10–12]. With an increase in SRA content, shrinkage is gradually reduced, and autogenous shrinkage is more significantly affected [13,14]. Studies on the mechanism of SRA show that as a surfactant, SRA is adsorbed on the surface of the pore solutions, reduces the surface tension at the interface, and lowers the pore tension generated by water consumption in pores [15–18], thereby decreasing the shrinkage stress. SRA can also delay hydration and change the morphology of hydration products [14,19]. The drying shrinkage mechanism of the cement mortar changes with the relative humidity (RH). When RH is low, the main factor identified is separation pressure; otherwise, the main factor is capillary stress. At this time, the evaporation of water in the pores causes the tension of the capillary wall to increase, resulting in shrinkage. With an increase in humidity, the capillary tension in the pores disappears, and shrinkage decreases again [20]. SRA can maintain the RH by increasing the viscosity of the pore solution [21]. However, SRA also negatively affects the strength development of cement [22].

At present, SRA is mostly used to reduce shrinkage deformation of high-performance concrete and alkali-excited slag cement [15,17]. The behavior of SRA in M-S-H cement has not been studied, and its mechanism of action remains unclear. Therefore, in the current study, the deformation of M-S-H cement with SRA was explored by shrinkage testing, and the mechanism was analyzed by surface tension testing, hydration heat testing, thermogravimetric analysis, and pore structure testing. This technique is expected to significantly help control shrinkage in M-S-H cement, thereby promoting its practical applications and providing support for reducing carbon emissions.

## 2. Materials and Methods

### 2.1. Materials

In this experiment, the materials mainly included lightly burned MgO (Xingtai, China) and silica fume (940U, Elkem Materials Ltd., Shanghai, China). The chemical compositions of these materials are listed in Table 1. The chemical composition data of MgO are from Xinhu Metal Materials Co., Ltd. (Xingtai, China), and the data of silica fume are from Elkem Materials Ltd. (Shanghai, China). Quartz sand is produced from the Xinlian quartz sand mine in Zhuanghe, Liaoning Province, with a particle size of 0.21–0.36 mm. Sodium hexametaphosphate is an analytically pure chemical reagent produced by China National Pharmaceutical Group Co., Ltd., Beijing, China. SRA adopts an alkyl polyether organic substance, which is SRA (I) from SBT New Material Co., Ltd., Nanjing, China.

**Table 1.** Chemical compositions of the raw materials (wt.%).

Material Type (wt.%)	MgO	SiO <sub>2</sub>	CaO	Al <sub>2</sub> O <sub>3</sub>	Fe <sub>2</sub> O <sub>3</sub>	K <sub>2</sub> O	P <sub>2</sub> O <sub>5</sub>	Na <sub>2</sub> O	SO <sub>3</sub>	Cl
MgO	97.41	0.56	1.93	0.03	0.03	-	-	-	0.02	0.02
Silica fume	0.89	95.20	0.44	1.04	0.27	1.23	0.18	0.33	0.42	-

### 2.2. Specimen Preparation

The experimental mixing ratios are listed in Table 2. In the table, SF stands for silica fume, SHMP for sodium hexametaphosphate, and SRA for shrinkage-reducing admixture. During the test, the raw materials were first weighed accurately in accordance with the mixing ratio. Second, SHMP and SRA were dissolved in the water and stirred evenly. Third, the lightly burned MgO and silica fume were mixed evenly by mechanical stirring, and the

mixing solution was added. Fourth, the cement mortar was mixed and stirred slowly for 120 s, followed by rapid mixing for 120 s for each mixing. Subsequently, quartz sand was added, and stirring continued to produce the mortar. Last, the mortar was poured into a steel mold. The sample was then cured at  $20 \pm 1$  °C and 95% RH for 24 h. Subsequently, the samples were cured in a curing box at  $20 \pm 3$  °C and RH at  $50 \pm 4\%$  until the specified age was reached. The strength test samples were then cured at  $20 \pm 1$  °C and 95% RH until the specified age was reached. The M-S-H cement paste was simultaneously prepared using the following ratios for the hydration heat and microscopic tests. For all tests, three samples were prepared, and the average value was considered the test result.

**Table 2.** Mix proportion of M-S-H mortars.

Binder	MgO/g	SF/g	Sand/g	Water/g	SHMP/g	SRA/g
J0	240	360	600	330	12	0
J1	240	360	600	330	12	6
J2	240	360	600	330	12	12
J3	240	360	600	330	12	18

### 2.3. Dry Shrinkage Test

M-S-H cement mortar specimens measuring 25 mm × 25 mm × 280 mm were prepared in accordance with Chinese JC/T603-2004 (standard test method for drying shrinkage of mortar) [23]. The molds were released after curing for 24 h in a standard environment. Subsequently, the specimens were placed in water for 24 h. Surface moisture and impurities on the copper measuring head were removed with a wet cloth, and a comparator (accuracy: 0.001 mm) was used to determine the initial reading. After the initial length was determined, the specimen was placed in a curing box ( $20 \pm 3$  °C,  $50 \pm 4\%$  RH) for curing. The specimen was then taken out. At the specified age, the specimen was removed to measure its length. The drying shrinkage rate and Water-Loss rate were calculated using the following equation:

$$\varepsilon_{st} = \frac{L_0 - L_t}{250} \times 100\%, \quad (1)$$

$$M_t = \frac{m_0 - m_t}{m_0} \times 100\%, \quad (2)$$

where  $\varepsilon_{st}$  is the drying shrinkage rate at  $t$  (d) age (%);  $L_0$  is the initial reading of the specimen length (mm);  $L_t$  is the length reading measured at  $t$  (d) age (mm);  $M_t$  is the Water-Loss rate at  $t$  (d) age (%);  $m_0$  is the initial mass of the specimen (g); and  $m_t$  is the mass measured at  $t$  (d) age (g).

### 2.4. Autogenous Shrinkage Test

First, the M-S-H cement mortar specimen measuring 25 mm × 25 mm × 280 mm was prepared and cured in the standard environment for 24 h before release. Impurities on the copper measuring head at both ends were removed, and the initial reading was measured using the comparator. Subsequently, the specimen was wrapped in two layers using aluminum foil, and then glued and placed together with the drying shrinkage specimen. At the specified age, the specimen was removed to measure its length. The autogenous shrinkage rate is calculated using the following equation:

$$\varepsilon_s = \frac{L_0 - L_t}{250} \times 100\%, \quad (3)$$

where  $\varepsilon_s$  is the autogenous shrinkage rate at  $t$  (d) age (%).  $L_0$  and  $L_t$  have the same meaning as Equation (1).

### 2.5. Internal Relative Humidity Test

The deformation of cement is closely related to its internal relative humidity. In this study, a Swiss Rotronic temperature–humidity sensor (model HL-NT3-D) and a HygroClip 2 (HC2) digital temperature–humidity probe with an accuracy of  $\pm 0.8\%$  were used to measure the relative humidity (RH) of the mortar. Its humidity range is 0–100%. The size of the specimen used in the test is 70.7 mm  $\times$  70.7 mm  $\times$  70.7 mm (Figure 1). The forming and curing conditions of the specimen were similar to those of the shrinkage experiment, and the test interval was set to 1 h.



**Figure 1.** Internal relative humidity test specimen under sealed condition.

### 2.6. Mechanical Properties Test

In accordance with the national standard GB/T 17671-1999 (Test method of cement mortar strength (ISO method)) [24], the strength of the specimen was determined using a pressure testing machine (WHY-300/10) controlled by a microcomputer (Shanghai Hualong Company, Shanghai, China). The test accuracy for compressive strength was 0.1 kN, and that for flexural strength was 0.1 N. Three 40 mm  $\times$  40 mm  $\times$  40 mm M-S-H mortar samples were subjected to compressive testing at a loading rate of 2400 N/S, and three 160 mm  $\times$  40 mm  $\times$  40 mm M-S-H mortar samples were subjected to three-point bending tests at a loading rate of 50 N/S and a span length of 100 mm.

### 2.7. Surface Tension Test

The surface tension measurements of the SRA and simulated pore solutions with different concentrations were determined using a K100C surface tensiometer (Kruss, Germany). The test accuracy was 0.01 mN/m. The test results were averaged among the three sets of tests, which was accurate to 0.1 mN/m. The surface tension of different solutions was measured by experiments, and the relationship between surface tension and capillary pressure was analyzed according to Equation (4) [25,26]:

$$\sigma_{cap} = \frac{2\gamma \cos(\theta)}{r}, \quad (4)$$

where  $\sigma_{cap}$  is the capillary pressure (MPa);  $\gamma$  is the surface tension of the pore solution (N/m);  $\theta$  is the contact angle; and  $r$  is the critical pore radius (m).

### 2.8. Hydration Heat Test

The hydration exothermic rate of hydration and the total hydration heat release in a span of 3 d from mixing raw materials to the hydration reaction were measured with a Tam Air III cement hydration microcalorimeter (TA Instrument, New Castle, DE, USA). The test sample was an M-S-H cement paste. The operating temperature range of the instrument

was 5–90 °C, and the accuracy was  $\pm 0.02$  °C. Subsequently, 8-channel rapid determination could be performed.

## 2.9. Microscopic Tests

### 2.9.1. Thermogravimetry Test

A TGA-DSC type 1 synchronous thermal analyzer (Mettler Toledo, Zurich, Switzerland) was used for testing. The main working parameters of the instrument were as follows: balance sensitivity, 0.01  $\mu\text{g}$ ; material, alumina crucible; measurement temperature range, room temperature to 1300 °C; temperature rise rate, 10 °C/min; and testing atmosphere,  $\text{N}_2$ . The M-S-H cement paste samples were ground in a standard test environment (20 °C, 60% RH), placed in a drying oven, dried to constant weight, sieved with a standard 0.075 mm sieve, and collected via a sealed bottle for testing.

### 2.9.2. Pore Structure Test

The pore structure of M-S-H cement paste was evaluated using the AutoPore IV 9500 MIP (Micromeritics, Norcross, GA, USA). The pore size was tested from 50 Å to 360  $\mu\text{m}$ . After sampling, the sample was immediately soaked in ethanol for more than 24 h to stop hydration and dehydration, and then left to air-dry to allow the ethanol to fully evaporate. The sample was placed in a vacuum-drying oven at 50 °C for 48 h. The baked sample was ultimately transferred into the glass tube of the dilatometer for measurement.

## 3. Results and Discussion

### 3.1. Dry Shrinkage and Water-Loss Rate

As shown in Figure 2, the drying shrinkage rate of the M-S-H mortar increased rapidly in the early stages (from the beginning of the test to day 7) and gradually stabilized over time. The incorporation of SRA inhibited drying shrinkage. With increasing content, the drying shrinkage gradually decreased. On day 28, drying shrinkage in the J3 group decreased by 22.6% relative to that in the J0 group. SRA reduced the surface tension of the pore solution to reduce the sensitivity of the capillary wall to water loss. The decrease in pore tension caused by water consumption decreased drying shrinkage.

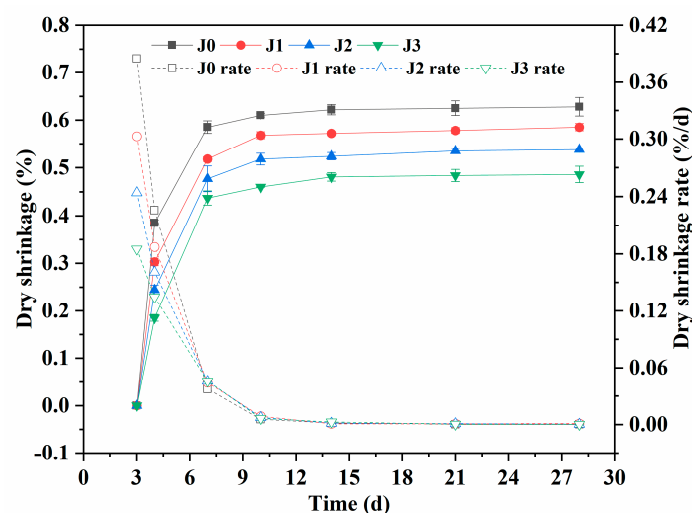


Figure 2. Dry shrinkage and shrinkage rate of M-S-H mortar with SRA.

As shown in Figure 3, the Water-Loss rate increased rapidly with age and gradually stabilized, most significantly within the first 7 days. This observation indicates that M-S-H mortar has poor water retention [27,28]. This pattern of change is consistent with that of drying shrinkage, likely because of the rapidly decreasing difference in humidity between the inside and the outside, as well as the blocking effect of  $\text{Mg}(\text{OH})_2$  microcrystals generated in the early stages on the connecting channel. Moreover, the incorporation of SRA

increases the Water-Loss rate and is positively correlated with the content. After day 28, the Water-Loss rate in the J3 group was 10% higher than that in the J0 group. The reason may be that SRA can reduce the saturation of the solution and accelerate the evaporation rate of water [29]. In addition, SRA has a certain air-entraining effect, and the gas introduced in the cement mixing process increases the channel for the outward migration of internal water, promoting the increase in water loss.

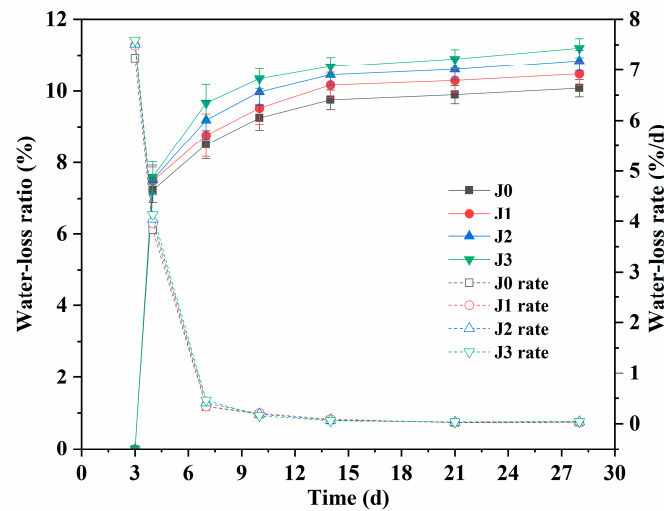


Figure 3. Water-Loss ratio and Water-Loss rate of M-S-H mortar with SRA.

As shown in Figure 4, the curves have two stages [30]: (i) the first stage has a duration of 0–3 d, characterized by a high rate of water loss under dry curing conditions, and (ii) the second stage ranges from 3–28 d; during this period, drying shrinkage increases linearly with water loss. In the initial stages of drying, water evaporation from the sample is mainly attributed to the large pores. Therefore, the slope of the curve is defined as a hydrous compressibility factor (CF) [31,32], representing the evolution of drying shrinkage and water loss. Thus, a lower CF indicates a smaller drying shrinkage with the same water loss, which is conducive to reducing shrinkage. The smallest CF is observed in the J3 group samples, indicating that the reduction effect is optimal when the SRA content is 3.0%.

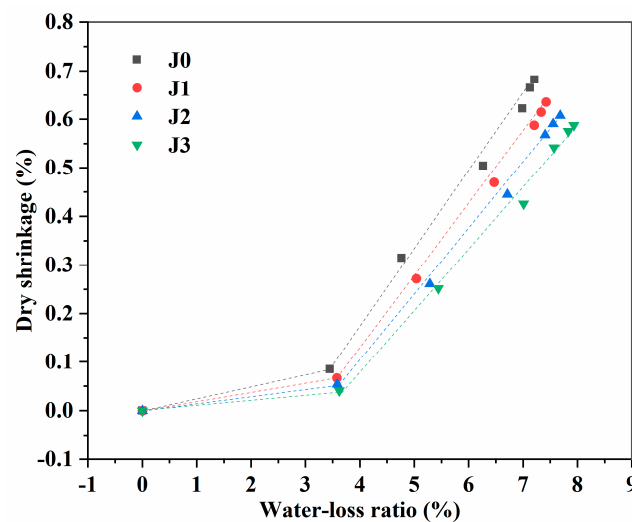
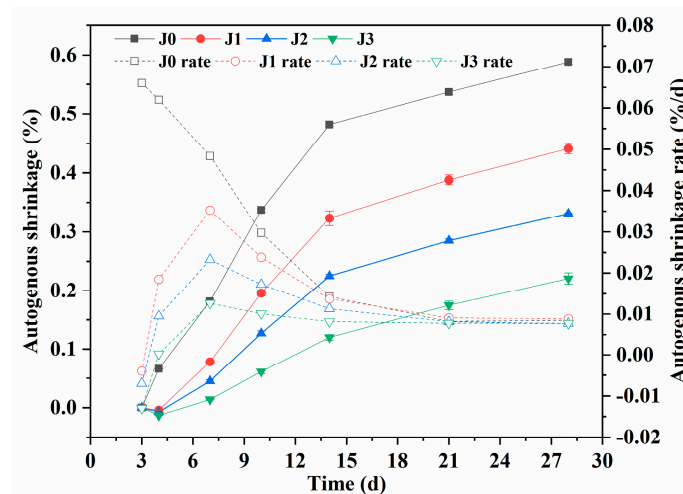


Figure 4. Relationship between dry shrinkage and Water-Loss ratio.

### 3.2. Autogenous Shrinkage and Relative Humidity

Owing to the constant water consumption during cement hydration, the autogenous shrinkage of cement occurs with a decreasing macroscopic volume. Consequently, contin-

uous water loss occurs in the internal capillary pores. As shown in Figure 5, autogenous shrinkage increases with curing time. The reason is that the mortar specimen is in a sealed state, and a large amount of water is consumed during the hydration reaction. A decrease in internal relative humidity and a continuously refined pore structure can generate considerable capillary pressure inside the mortar, resulting in significant autogenous shrinkage [33]. However, autogenous shrinkage was significantly reduced in the presence of SRA. The higher the dosage of SRA, the better the reduction effect. On day 28, autogenous shrinkage in the J3 group was reduced by 60% relative to that in the J0 group. SRA can decrease the capillary wall pressure caused by water consumption during hydration. As the hydration proceeds, the water in the pores is constantly consumed, increasing the concentration of SRA and significantly reducing the surface tension. Moreover, the M-S-H mortar mixed with SRA slightly expanded within 3 d. The reason is that in early hydration, SRA reduced the surface energy of the M-S-H gel. These decreases delayed hydration and generated more  $Mg(OH)_2$  than that in the J0 group, leading to a certain volume expansion [34].



**Figure 5.** Autogenous shrinkage and shrinkage rate of M-S-H mortar with SRA.

SRA can significantly delay the reduction of internal RH, as shown in Figure 6. Internal relative humidity in the J3 group on day 28 was 82.0%, which is higher than that in the J0 group (77.0%). Decreases in the internal relative humidity in the J0 group and in the J3 group were observed near 36 h and near 60 h, respectively. These reductions suggest that SRA can also delay early hydration in M-S-H mortar, and this effect lasts for about 1 d, further reducing the ability to consume water. Therefore, SRA can effectively preserve the humidity inside the M-S-H mortar, alleviate self-drying caused by hydration, and reduce the capillary tension inside the mortar to decrease the autogenous shrinkage of the M-S-H mortar [35]. SRA is a surfactant; thus, the hydrophilic group in its molecular chain can bind part of the water in the cement pores. Consequently, this part of bound water is adsorbed near the SRA molecules and no longer participates in hydration to be consumed. With an increase in SRA concentration, the number of SRA molecules in the capillary solution increases, and incorporating more water causes the humidity in the mortar to rise [36].

The internal RH and autogenous shrinkage of the M-S-H cement exhibits a good linear relationship, similar to that of high-strength concrete with a low water–cement ratio [37], as shown in Figure 7. As SRA dosage rises (seen in Figure 7 from J0 to J3), the slope of the fitting curve decreases, indicating that SRA can attenuate the sensitivity of autogenous shrinkage to internal RH.

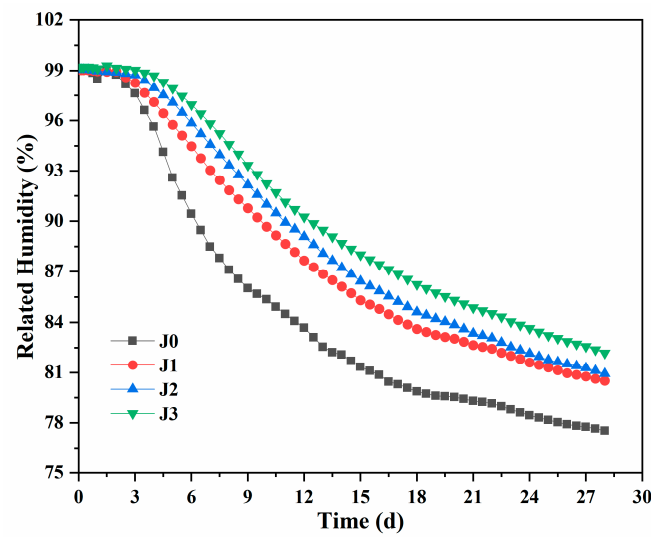


Figure 6. Internal relative humidity of M-S-H mortar with SRA.

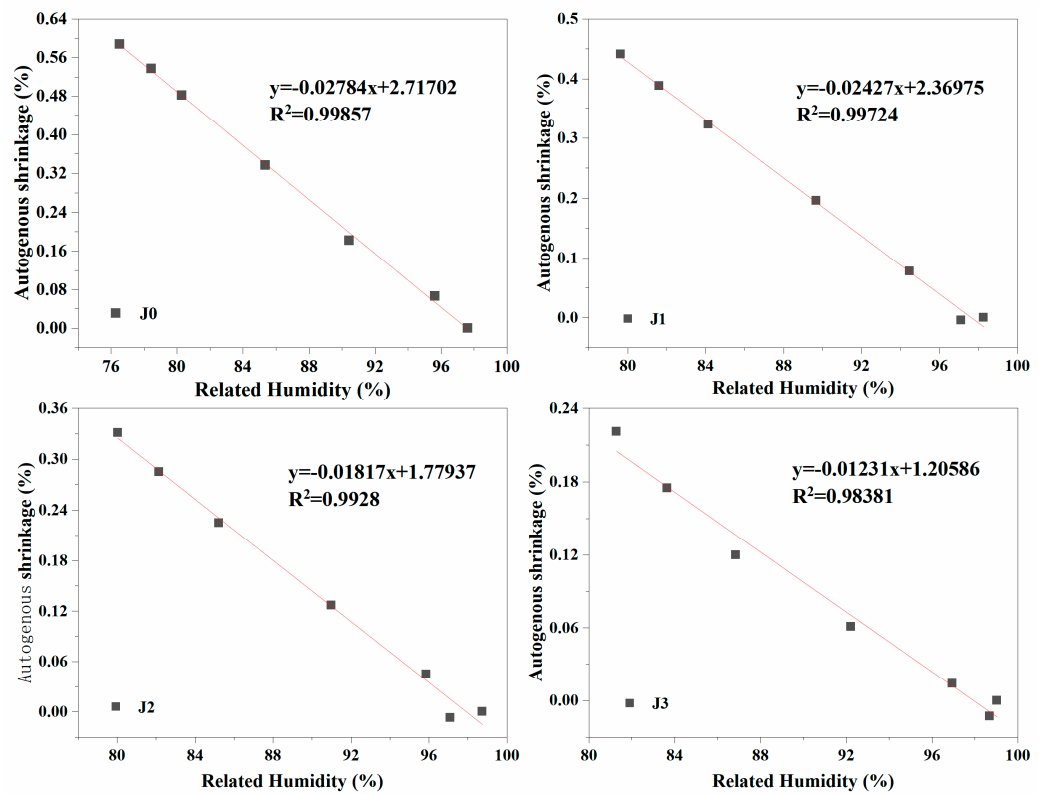


Figure 7. Relationship between RH and autogenous shrinkage of M-S-H mortar.

### 3.3. Mechanical Properties

The adverse influence of SRA on mechanical properties limits its application in practical engineering. The compressive strength of M-S-H mortar increases with age; similarly, the flexural strength is also enhanced but only slightly, as shown in Figure 8. These strengths are significantly reduced by SRA, but the change in content only slightly affects the compressive strength. The reason is that SRA increases porosity, which increases the internal defects of the mortar. Compressive strength in the J3 group on days 3, 7, and 28 decreased by 37.5%, 31.6%, and 28.4%, and flexural strength decreased by 28.5%, 20.9%, and 20.3%, respectively. Therefore, as the age increased, the adverse effect was gradually reduced.

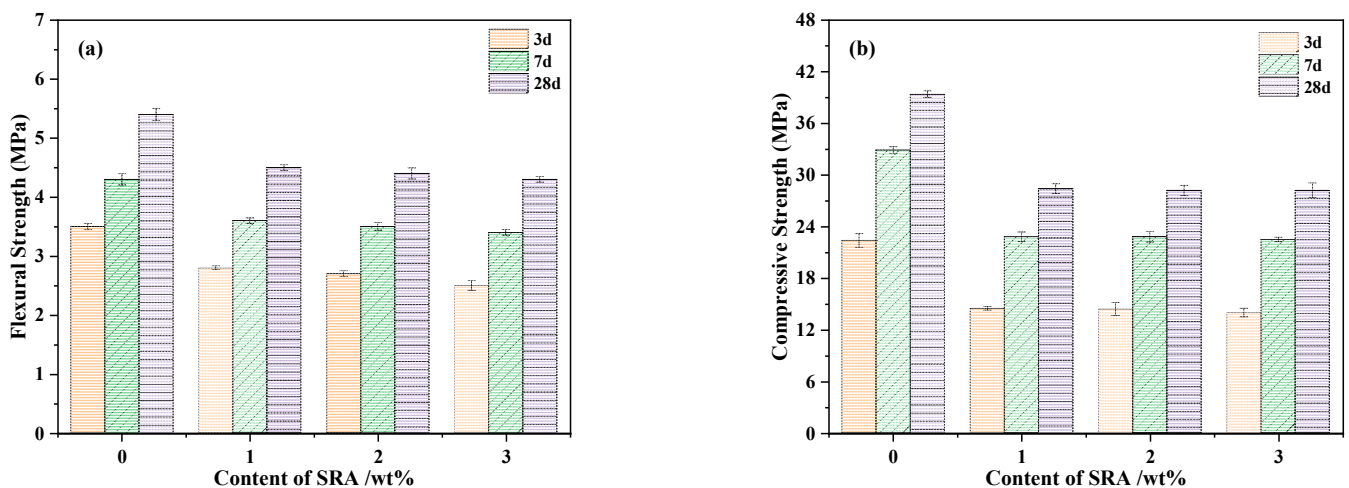


Figure 8. (a) Flexural strength and (b) compressive strength of M-S-H mortar with SRA.

### 3.4. Surface Tension

As a type of surfactant, SRA can reduce the surface tension of the solution. This characteristic of SRA is generally manifested in two respects: (i) the ability to reduce the surface tension, i.e., to minimize the surface tension of the solvent, and (ii) the efficiency of reducing the surface tension, i.e., the maximum SRA concentration that needs to be achieved when the surface tension is reduced to the minimum [27].

With its high cost considered, SRA needs to be limited to a lower concentration during application to improved its shrinkage effect. Therefore, the surface tension of SRA in different solvents was evaluated within a lower concentration range (Figure 9). Obtaining the pore solution for testing via in situ extrusion presented a challenge because of the small amount of pore solution in M-S-H mortar. Existing research results have shown that the pore solution of M-S-H mortar with a high water–cement ratio is consistent with that of a low water–cement ratio. Therefore, M-S-H mortar with a high water–cement ratio ( $W/C = 10$ ) was prepared to replace the actual cement for testing [38]. As shown in the figure, SRA can significantly reduce the surface tension of distilled water. When SRA content is only 1.0%, the surface tension can be reduced by 19.0% relative to that of the control group. The reducing ability of SRA on the surface tension of simulated pore solution is less than that of distilled water. With an increase in SRA content, the surface tension decreases and tends to be smooth, and the decreasing effect gradually weakens. SRA can reduce the sensitivity of capillary pores to water by reducing the surface tension of the pore solution, thus impeding the development of capillary tension and shrinkage stress caused by water consumption.

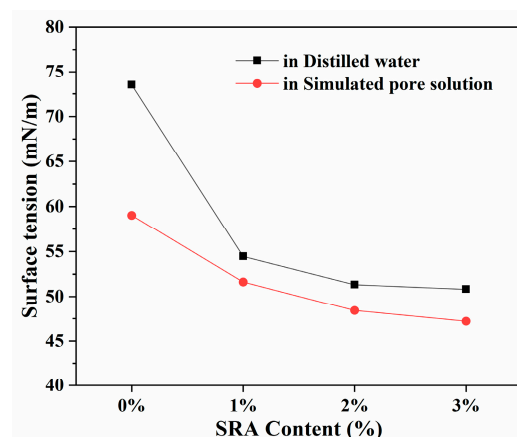
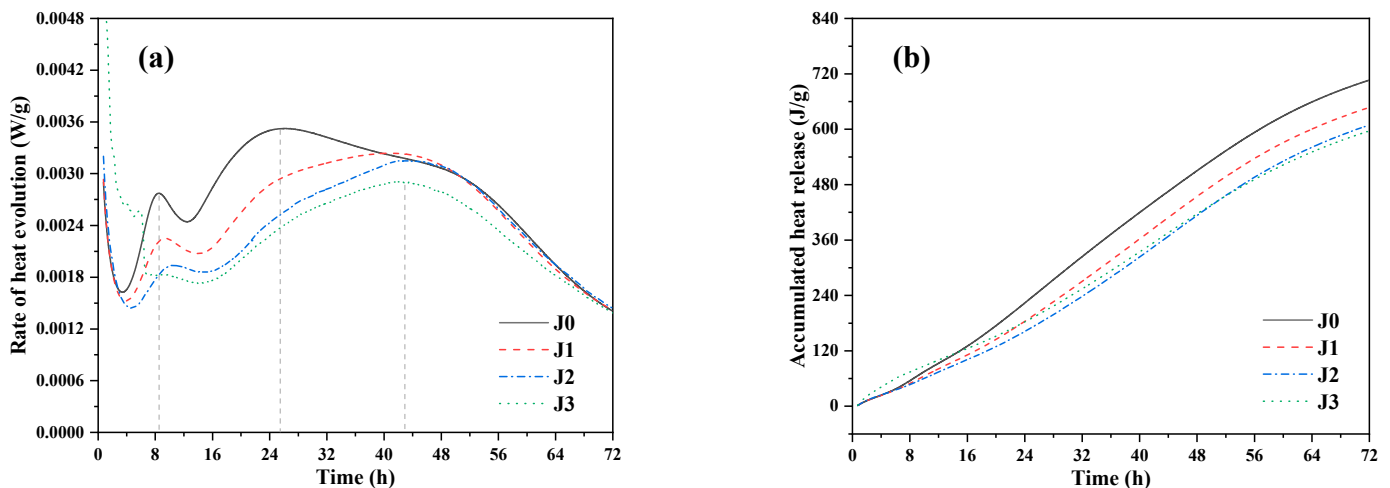


Figure 9. Effect of SRA on the surface tension of water and simulated pore solution.

### 3.5. Hydration Heat

Figure 10 presents the hydration heat curve of the M-S-H cement with SRA. The first exothermic peak appears at the 8.5 h time point of the hydration reaction, which is primarily driven by the exothermic heat released during the wetting and dissolution of MgO and silica fume. After continued hydration for about 25 h, the heat release reaches a second peak, which is mainly attributed to the formation of  $\text{Mg}(\text{OH})_2$  and M-S-H gel, before gradually decreasing. The M-S-H cement paste containing SRA showed a lower peak heat release in the first stage, which may be due to the adsorption of SRA on the surface of MgO and silica fume particles, and the hydrophobic group in the tail of SRA prevented their contact with water [36]. Compared with the J0 group, the presence of SRA prompted the second exothermic peak to shift backward and occur after the hydration reaction reached 43 h, which indicates that SRA caused a delay in the early hydration [22,39]. The reason is that SRA can attach to the hydration products, preventing them from participating in further hydration reactions. Moreover, as the SRA content increased, the peak value of the hydration heat decreased, indicating a reduction in the degree of hydration. This process, in turn, reduced the self-desiccation caused by early hydration and ultimately decreased the shrinkage of M-S-H cement [40,41]. Its lower release of hydration heat also reduced the temperature difference within the cement, which then lowered the risk of cracking [42,43]. In addition, the adjustment of the hydration process by SRA also delayed the decrease in the humidity in cement.



**Figure 10.** (a) Hydration exothermic rate and (b) total hydration heat release of M-S-H cement with SRA.

### 3.6. Thermogravimetric Analysis

The weightlessness process of the M-S-H cement was mainly divided into three stages, as shown in Figure 11. The first stage was 50–250 °C, which is mainly the removal of free water in tiny pores and physically adsorbable water in gel pores, among which the adsorbable water was mainly removed between 105–250 °C [44]. The gel water content in the J0 group increased with the hydration reaction, indicating that the pore size was gradually refined, and the gel phase content increased. The weight-loss valley near 100 °C in the J3 group was smaller than that in the J0 group because SRA delayed the hydration and produced less M-S-H gel phase in hydration products.

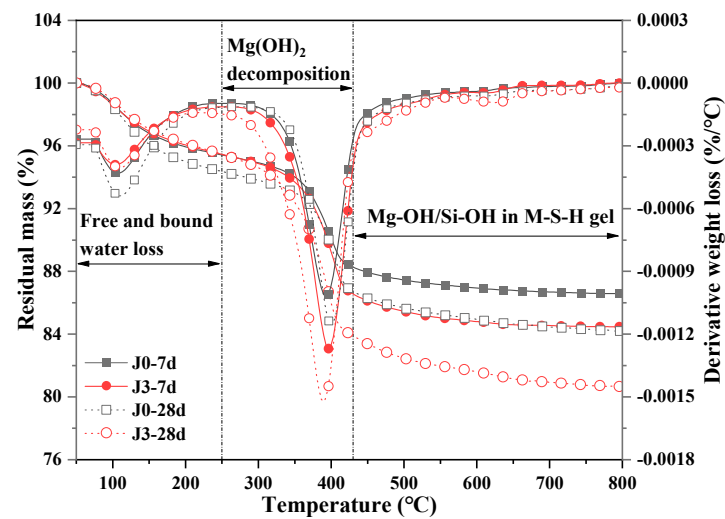


Figure 11. TG and DTG curves of M-S-H cement with SRA under dry conditions.

The second stage was 250–430 °C mainly due to the thermal decomposition of  $\text{Mg}(\text{OH})_2$  [4,45]. At 400 °C, the weight-loss valley of both groups increased with time, indicating that the  $\text{Mg}(\text{OH})_2$  content increased gradually. Owing to the rapid increase in the concentration of  $\text{Mg}^{2+}$  and  $\text{OH}^-$  ions in the pore solution under rapid Water-Loss conditions in the dry environment, the supersaturation of  $\text{Mg}(\text{OH})_2$  crystal increased, prompting the formation and precipitation rates to exceed the consumption rate. However, the  $\text{Mg}(\text{OH})_2$  content in the J3 group exceeded that in the J0 group. SRA reduced the polarity of water, leading to a lower ionic solubility, as well as accelerated the formation of  $\text{Mg}(\text{OH})_2$ . Moreover, SRA may be adsorbed on  $\text{Mg}(\text{OH})_2$  crystal, hindering a further reaction.

The third stage was 430–800 °C, which mainly corresponded to the release of  $\text{Mg-OH}$  and  $\text{Si-OH}$  in the M-S-H gel [45]. In the figure, a small weightless valley can be seen near 650 °C, which is due to the thermal decomposition of  $\text{MgCO}_3$  generated by the carbonization reaction during the curing process. With an increase in curing age, the degree of carbonization also increased. Therefore, under dry conditions, SRA can delay the hydration rate and increase the content of  $\text{Mg}(\text{OH})_2$  crystals. Thus, the expansion strain generated by the crystallization pressure of  $\text{Mg}(\text{OH})_2$  compensates for part of the shrinkage strain [46].

The weight-loss process of M-S-H cement under sealed conditions is similar to that under dry conditions, and the process comes in three stages, as shown in Figure 12. In the first stage, the weight-loss valley near 100 °C increased as the curing age increased and was more significant than that under dry conditions. Under sealed conditions, water inside the M-S-H sample is entirely used for its hydration reaction, hence the higher hydration rate than that under dry conditions. Thus, more gel phases are generated and more gel water is adsorbed. However, SRA delays the hydration rate, hence the lower gel water content in the J3 group than in the J0 group. In the second stage, the weight-loss valley of both groups near 400 °C decreased with time, indicating that the  $\text{Mg}(\text{OH})_2$  content gradually decreased under sealed conditions, which was consistent with the change in the M-S-H gel phase. This reduction suggests that SRA delays the conversion from  $\text{Mg}(\text{OH})_2$  to M-S-H gel. The weightlessness valley disappeared near 650 °C because the samples were isolated from the outside world under sealed conditions; thus, no  $\text{MgCO}_3$  was generated. Under sealed conditions, SRA can reduce autogenous shrinkage by reducing the hydration rate and delaying the reduction of humidity in the cement [16].

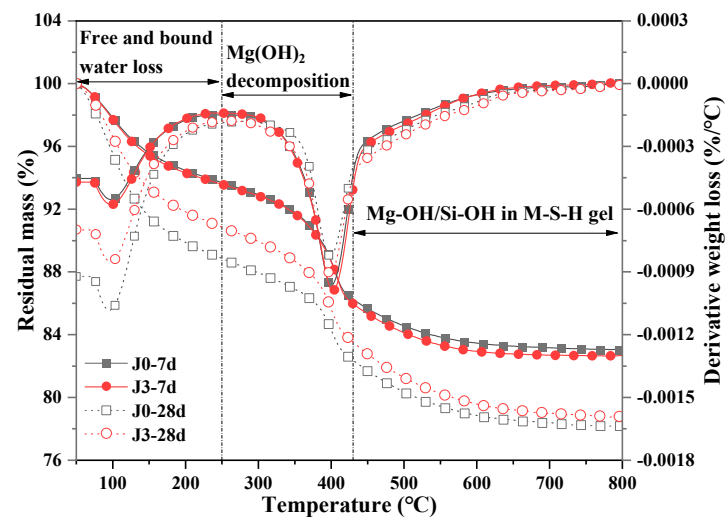


Figure 12. TG and DTG curves of M-S-H cement with SRA under sealed conditions.

### 3.7. Pore Structure Analysis

The pore structure largely influenced the shrinkage properties of M-S-H cement. The pores <50 nm in the cement-based material only slightly affect mechanical properties; meanwhile, the capillary pressure caused by water loss is greater, and the shrinkage stress is greater. Studies have shown that SRA can improve the pore size distribution of cement-based materials [47]. SRA solution would remain in the pores and reduce the contractile strain by affecting the interaction potential energy between capillary walls [48]. With the continuous hydration reaction under dry conditions, the pore (>50 nm) volume in the J0 group decreased significantly, and the pore size tended to be refined on day 28, as shown in Figure 13a. In addition, the total porosity decreased (Figure 13b) as a result of the continuous generation of the gel phase, which filled the large pores in the paste.

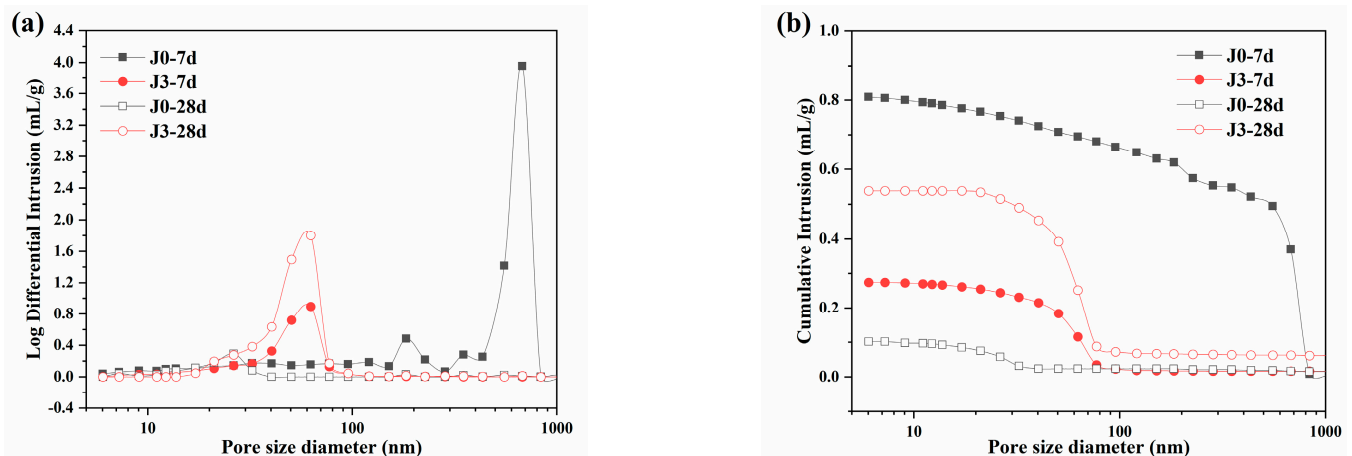


Figure 13. (a) Pore size distribution and (b) cumulative pore volume of M-S-H cement with SRA under dry conditions.

On day 7, pores of diameter above 100 nm in the J0 group occupied 80% of the pore volume. In the early stages of hydration, the sample exhibited severe dehydration, and the hydration products showed poor strength, hence the presence of numerous macropores in the internal structure and large shrinkage deformation. On day 7, mass  $\text{Mg}(\text{OH})_2$  crystals precipitated because of water loss, generating extrapolated pressure on the pore wall and preventing the further collapse of the pore structure. On day 28, the 50–100 nm pores were completely filled with hydration products. However, the porosity of samples in the J3 group increased with the hydration reaction, which was mainly manifested by an increase

in pore volume of 40–70 nm. The macropore (>100 nm) volume increased most significantly. SRA lowered the hydration rate, resulting in smaller pores generated by hydration on day 7 than in the control group, but also promoting the loss of water. The total porosity on day 28 is considerably higher, which is also reported in other studies [49,50]. However, the coarser pore size also led to a decrease in compressive strength.

SRA increased the average pore radius and the proportion of macropores. According to the Young–Laplace Equation (4), the capillary tension was negatively correlated with the pore radius. Consequently, the capillary tension was further decreased, suggesting that the reduction of shrinkage is influenced by reducing the surface tension and coarsening the pore size [18].

With the hydration reaction, the pore development of samples in the J0 group is similar to that under dry conditions, in which pore refinement mainly results from continuous hydration, as shown in Figure 14. After being sealed for 28 d, the macropores (>100 nm) in the J0 group were gradually filled with hydration products and then disappeared, and the 10–50 nm pores increased. Autogenous shrinkage arising from self-drying increased. With the hydration reaction, the pore size distribution of the J3 group shifted to the right. Both the macropores (>100 nm) and porosity increased. However, the pore (10–100 nm) volume was almost unchanged, and only the coarsening of the pore size was observed. SRA increased the 10–50 nm pores in the paste, and macropores (>100 nm) were still observed on day 28. Overall porosity was considerably higher than that in the J0 group, that is consistent with the decrease in compressive strength. The M-S-H gel is denser in the early stages because SRA decreases the hydration rate. The pores generated by hydration were fewer than those in the J0 group, and the porosity was lower on day 7.

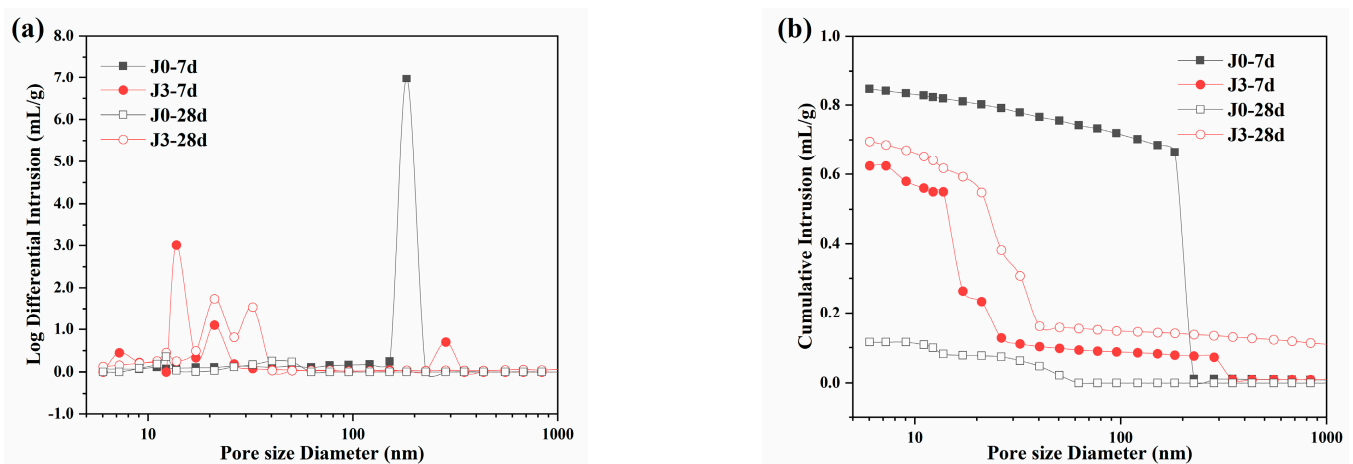


**Figure 14.** (a) Pore size distribution and (b) cumulative pore volume of M-S-H cement with SRA under sealed conditions.

In accordance with the Young–Laplace Equation (4), the smaller the pore sizes, the higher the capillary tension, resulting in greater shrinkage stress. Therefore, SRA can reduce autogenous shrinkage not only by improving the porosity but also by increasing the volume of macropores to reduce the capillary tension caused by pores [34].

#### 4. Conclusions

The deformation of M-S-H cement with a polyether SRA was evaluated. The mechanism of SRA was examined by surface tension testing, hydration heat testing, thermogravimetric analysis, and MIP. The major conclusions are as follows.

1. For M-S-H cement, its drying shrinkage first increases and is then stabilized as age increases. SRA can reduce drying shrinkage, but the effect of dosage is not significant. At 28 d, the drying shrinkage of M-S-H mortar can be reduced by 22.6% at most. In addition, SRA can also delay the hydration rate by inhibition of  $Mg(OH)_2$  precipitated

- out of the pore solution because of supersaturation, and the expansion strain generated by crystallization pressure compensates for part of the contraction strain.
2. For M-S-H cement, its Water-Loss rate is the same as the rate of change in drying shrinkage. SRA can increase the Water-Loss rate because it can lower the polarity of the water solution, as well as reduce the saturation of the solution to accelerate evaporation. At 28 d, the Water-Loss rate can be increased by 10% at most. SRA can also coarsen the pore size and increase the porosity, thus promoting water loss. In addition, SRA exerts a certain air entrainment effect, and the gas introduced during the cement mixing process increases the channel for the outward migration of internal water, promoting an increase in water loss.
  3. For M-S-H cement, its autogenous shrinkage exhibits continuous growth with an increase in age. In the presence of SRA, autogenous shrinkage is reduced, and slight expansion occurs in the early stages. When the dosage of SRA is 3%, autogenous shrinkage can be reduced by about 60% at 28 d. The reduction in shrinkage can be improved with an increase in dosage. In addition, SRA can increase the volume of macropores to reduce the capillary tension.
  4. For M-S-H cement, the internal humidity decreases gradually and tends to become stable with an increase in age. This reduction can be delayed by SRA and improved by an increase in dosage. The internal humidity in M-S-H mortar with 3% SRA content began to decrease at about 60 h, and remained at 82% at 28 d, higher than the 77% in the control group. This also indicates that SRA can maintain its internal relative humidity and reduce the capillary tension generated by water consumption to alleviate self-drying.
  5. For M-S-H cement, the strengths increased gradually with an increase in age. However, SRA exerts a weakening effect on strength, and this adverse effect gradually decreases as age increases. At 28 d, the compressive strength and flexural strength of M-S-H mortar with 3% SRA content decreased by 28.4% and 20.3%, respectively. SRA increases the porosity and the volume of macropores, leading to an increase in defects in the paste.

It can be seen that SRA can effectively slow the volume deformation of M-S-H cement under dry and sealed conditions. However, the behavior of SRA in the pore solution of M-S-H cement has not been studied. Therefore, it is necessary to study the changes in ion concentration and pH in M-S-H cement pore solution with SRA at different ages, so as to further clarify the mechanism of SRA. This will facilitate the application of SRA in M-S-H cement.

**Author Contributions:** Conceptualization, J.H.; formal analysis, T.Z.; funding acquisition, T.Z.; investigation, H.F. and J.H.; resources, T.Z.; writing—original draft, H.F.; writing—review and editing, J.H. All authors have read and agreed to the published version of the manuscript.

**Funding:** This research was funded by the National Natural Science Foundation of China (52178189) and Liaoning Revitalization Talents Program (XLYC2007126).

**Data Availability Statement:** All data, models, and code generated or used during the study appear in the submitted article.

**Conflicts of Interest:** The authors declare no conflict of interest.

## References

1. Dan, Z. *Research on the Dry-Shrinkage, Mechanism and Influence Factors of Cement Mortar*; Chang'an University: Xi'an, China, 2015.
2. Zhang, T.; Cheeseman, C.; Vandeperre, L. Development of low pH cement systems forming magnesium silicate hydrate (M-S-H). *Cem. Concr. Res.* **2011**, *41*, 439–442. [[CrossRef](#)]
3. Li, Z.; Zhang, T.; Hu, J.; Tang, Y.; Niu, Y.; Wei, J.; Yu, Q. Characterization of reaction products and reaction process of MgO-SiO<sub>2</sub>-H<sub>2</sub>O system at room temperature. *Constr. Build. Mater.* **2014**, *61*, 252–259. [[CrossRef](#)]
4. Jin, F.; Al-Tabbaa, A. Thermogravimetric study on the hydration of reactive magnesia and silica mixture at room temperature. *Thermochim. Acta* **2013**, *566*, 162–168. [[CrossRef](#)]

5. Zhang, T.; Vandeperre, L.; Cheeseman, C. Magnesium-silicate-hydrate cements for encapsulating problematic aluminium containing wastes. *J. Sustain. Cem.-Based Mater.* **2012**, *1*, 34–45. [[CrossRef](#)]
6. Zhou, Z. *Influencing Factors and Mechanism of Volume Stability of Magnesium Silicate Hydrate System*; Dalian University of Technology: Dalian, China, 2022.
7. Zhang, T.; Liang, X.; Li, C.; Lorin, M.; Li, Y.; Vandeperre, L.J.; Cheeseman, C.R. Control of drying shrinkage in magnesium silicate hydrate (m-s-h) gel mortars. *Cem. Concr. Res.* **2016**, *88*, 36–42. [[CrossRef](#)]
8. Li, X.; Fu, Q.; Lv, Y.; Leng, D.; Jiang, D.; He, C.; Wu, K.; Dan, J. Influence of curing conditions on hydration of magnesium silicate hydrate cement. *Constr. Build. Mater.* **2022**, *361*, 129648. [[CrossRef](#)]
9. Wu, L.; Farzadnia, N.; Shi, C.; Zhang, Z.; Wang, H. Autogenous shrinkage of high performance concrete: A review. *Constr. Build. Mater.* **2017**, *149*, 62–75. [[CrossRef](#)]
10. Mehrnosh, A.; Tarik, O.; Nihat, K. Effect of microfibers or SRA on the shrinkage and mechanical properties of alkali activated slag/fly ash-based mortars incorporating recycled fine aggregate. *Constr. Build. Mater.* **2023**, *373*, 130883.
11. Ma, H.; Zhu, H.; Chen, H.; Ni, Y.; Xu, X.; Huo, Q. Shrinkage-reducing measures and mechanisms analysis for alkali-activated coal gangue-slag mortar at room temperature. *Constr. Build. Mater.* **2020**, *252*, 119001. [[CrossRef](#)]
12. Ye, H.; Fu, C.; Lei, A. Mitigating shrinkage of alkali-activated slag by polypropylene glycol with different molecular weights. *Constr. Build. Mater.* **2020**, *245*, 118478. [[CrossRef](#)]
13. Aghaee, K.; Sposito, R.; Khayat, K. Synergistic effect of shrinkage mitigating materials on rheological properties of flowable and thixotropic cement paste. *Cem. Concr. Compos.* **2022**, *133*, 104686. [[CrossRef](#)]
14. Makhadmeh, W.; Soliman, A. On the mechanisms of shrinkage reducing admixture in alkali activated slag binders. *J. Build. Eng.* **2022**, *56*, 104812. [[CrossRef](#)]
15. Zhang, W.; Lin, H.; Xue, M.; Wang, S.; Ran, J.; Su, F.; Zhu, J. Influence of shrinkage reducing admixture on the performance of cementitious composite: A review. *Constr. Build. Mater.* **2022**, *325*, 126579. [[CrossRef](#)]
16. Zhan, P.; He, Z. Application of shrinkage reducing admixture in concrete: A review. *Constr. Build. Mater.* **2019**, *201*, 676–690. [[CrossRef](#)]
17. He, Z.H.; Hu, H.B.; Casanova, I.; Liang, C.F.; Du, S.G. Effect of shrinkage reducing admixture on creep of recycled aggregate concrete. *Constr. Build. Mater.* **2020**, *254*, 119312. [[CrossRef](#)]
18. Li, C.; Wang, Q.; Chen, J.; Jia, S.; Jiang, L.; He, J. Effect of polyether-type SRA on the drying shrinkage, pore structure and properties of blended mortar incorporating limestone powder. *Constr. Build. Mater.* **2020**, *264*, 120173. [[CrossRef](#)]
19. Zhang, W.; Xue, M.; Lin, H.; Duan, X.; Jin, Y.; Su, F. Effect of polyether shrinkage reducing admixture on the drying shrinkage properties of alkali-activated slag. *Cem. Concr. Compos.* **2023**, *136*, 104865. [[CrossRef](#)]
20. Rahoui, H.; Maruyama, I.; Vandamme, M.; Pereira, J.M.; Mosquet, M. Impact of an SRA (hexylene glycol) on irreversible drying shrinkage and pore solution properties of cement pastes. *Cem. Concr. Res.* **2021**, *143*, 106227. [[CrossRef](#)]
21. Bessaies-Bey, H.; Baumann, R.; Schmitz, M.; Radler, M.; Roussel, N. Organic admixtures and cement particles: Competitive adsorption and its macroscopic rheological consequences. *Cem. Concr. Res.* **2016**, *80*, 1–9. [[CrossRef](#)]
22. Rajabipour, F.; Sant, G.; Weiss, J. Interactions between shrinkage reducing admixtures (SRA) and cement paste's pore solution. *Cem. Concr. Res.* **2008**, *38*, 606–615. [[CrossRef](#)]
23. *JC/T603-2004*; Standard Test Method for Drying Shrinkage of Mortar. China Building Materials Academy: Beijing, China, 2004.
24. *GB/T 17671-1999*; Test Method of Cement Mortar Strength (ISO Method). China Building Materials Academy: Beijing, China, 1999.
25. Radlinska, A.; Rajabipour, F.; Bucher, B.; Henkensiefken, R.; Sant, G.; Weiss, J. Shrinkage Mitigation Strategies in Cementitious Systems: A Closer Look at Differences in Sealed and Unsealed Behavior. *Transp. Res. Rec.* **2008**, *2070*, 59–67. [[CrossRef](#)]
26. Jia, Y. *The Effect of Na-HMP and CaO on the Reaction Mechanism of MgO-SiO<sub>2</sub>-H<sub>2</sub>O System*; Dalian University of Technology: Dalian, China, 2017.
27. Zhang, T.; Vandeperre, L.J.; Cheeseman, C.R. Formation of magnesium silicate hydrate (M-S-H) cement pastes using sodium hexametaphosphate. *Cem. Concr. Res.* **2014**, *65*, 8–14. [[CrossRef](#)]
28. Walling, S.A.; Kinoshita, H.; Bernal, S.A.; Collier, N.C.; Provis, J.L. Structure and properties of binder gels formed in the system Mg(OH)<sub>2</sub>-SiO<sub>2</sub>-H<sub>2</sub>O for immobilisation of Magnox sludge. *Dalton Trans.* **2015**, *44*, 8126–8137. [[CrossRef](#)]
29. Aitcin, P.; Flatt, R. *Science and Technology of Concrete Admixtures*; Woodhead Publishing: Sawston, UK, 2015.
30. Jaafri, R.; Aboulayt, A.; Alam, S.Y.; Roziere, E.; Loukili, A. Natural hydraulic lime for blended cement mortars: Behavior from fresh to hardened states. *Cem. Concr. Res.* **2019**, *120*, 52–65. [[CrossRef](#)]
31. Granger, L.; Torrenti, J.M.; Acker, P. Thoughts about drying shrinkage: Experimental results and quantification of structural drying creep. *Mater. Struct.* **1997**, *30*, 588–598. [[CrossRef](#)]
32. Benboudjema, F.; Meftah, F.; Torrenti, J.M. Interaction between drying, shrinkage, creep and cracking phenomena in concrete. *Eng. Struct.* **2005**, *27*, 239–250. [[CrossRef](#)]
33. Samouh, H.; Roziere, E.; Wisniewski, V.; Loukili, A. Consequences of longer sealed curing on drying shrinkage, cracking and carbonation of concrete. *Cem. Concr. Res.* **2017**, *95*, 117–131. [[CrossRef](#)]
34. Sant, G.; Lothenbach, B.; Juilland, P.; Le Saout, G.; Weiss, J.; Scrivener, K. The origin of early age expansions induced in cementitious materials containing shrinkage reducing admixtures. *Cem. Concr. Res.* **2011**, *41*, 218–229. [[CrossRef](#)]
35. Saliba, J.; Roziere, E.; Grondin, F.; Loukili, A. Influence of shrinkage-reducing admixtures on plastic and long-term shrinkage. *Cem. Concr. Compos.* **2011**, *33*, 209–217. [[CrossRef](#)]

36. Zhang, Z. *Single and Combined Effects of Shrinkage-Reducing Admixture and Internal Curing on Autogenous Shrinkage of Hardened Cement Pastes with Low Water-Cement Ratio*; Chongqing University: Chongqing, China, 2017.
37. Lura, P.; Jensen, O.M.; Breugel, K. P. Autogenous shrinkage in high-performance cement paste: An evaluation of basic mechanisms. *Cem. Concr. Res.* **2003**, *33*, 223–232. [[CrossRef](#)]
38. Adamson, A.; Klerer, J. Physical Chemistry of Surfaces. *J. Electrochem. Soc.* **1977**, *124*, 192C. [[CrossRef](#)]
39. Juilland, P.; Gallucci, E.; Flatt, R.; Scrivener, K. Dissolution theory applied to the induction period in alite hydration. *Cem. Concr. Res.* **2010**, *40*, 831–844. [[CrossRef](#)]
40. Soliman, A.; Nehdi, M. Effects of shrinkage reducing admixture and wollastonite microfiber on early-age behavior of ultra-high performance concrete. *Cem. Concr. Compos.* **2014**, *46*, 81–89. [[CrossRef](#)]
41. Maia, L.; Figueiras, H.; Nunes, S.; Azenha, M.; Figueiras, J. Influence of shrinkage reducing admixtures on distinct SCC mix compositions. *Constr. Build. Mater.* **2012**, *35*, 304–312. [[CrossRef](#)]
42. Scrivener, K.; Juilland, P.; Monteiro, P. Advances in understanding hydration of Portland cement. *Cem. Concr. Res.* **2015**, *78*, 38–56. [[CrossRef](#)]
43. Xu, G.; Tian, Q.; Miao, J.; Liu, J. Early-age hydration and mechanical properties of high volume slag and fly ash concrete at different curing temperatures. *Constr. Build. Mater.* **2017**, *149*, 367–377. [[CrossRef](#)]
44. Wei, J. *Research on MgO-SiO<sub>2</sub>-H<sub>2</sub>O System Cement and Its Hydration Mechanism*; China Building Materials Academy: Beijing, China, 2004.
45. Szczerba, J.; Prorok, R.; Śniezek, E.; Madej, D.; Maślona, K. Influence of time and temperature on ageing and phases synthesis in the MgO-SiO<sub>2</sub>-H<sub>2</sub>O system. *Thermochim. Acta* **2013**, *567*, 57–64. [[CrossRef](#)]
46. Cerulli, T.; Pistolesi, C.; Maltese, C.; Salvioni, D. Effects of shrinkage reducing admixtures on the physical mechanical properties of mortars. In Proceedings of the ICMA International Conference on Cement Microscopy, Albuquerque, NM, USA, 29 April 2001–4 May 2001; pp. 58–76.
47. Yang, G.; Wu, Y.; Li, H.; Gao, N.; Jin, M.; Hu, Z.; Liu, J. Effect of shrinkage-reducing polycarboxylate admixture on cracking behavior of ultra-high strength mortar. *Cem. Concr. Compos.* **2021**, *122*, 104117. [[CrossRef](#)]
48. Ribeiro, A.B.; Gonçalves, A.; Carrajola, A. Effect of shrinkage reduction admixtures on the pore structure properties of mortars. *Mater. Struct.* **2006**, *39*, 179–187. [[CrossRef](#)]
49. Zhang, W.; Hama, Y.; Na, S.H. Drying shrinkage and microstructure characteristics of mortar incorporating ground granulated blast furnace slag and shrinkage reducing admixture. *Constr. Build. Mater.* **2015**, *93*, 267–277. [[CrossRef](#)]
50. Ling, Y.; Wang, K.; Fu, C. Shrinkage behavior of fly ash based geopolymer pastes with and without shrinkage reducing admixture. *Cem. Concr. Compos.* **2019**, *98*, 74–82. [[CrossRef](#)]

**Disclaimer/Publisher’s Note:** The statements, opinions and data contained in all publications are solely those of the individual author(s) and contributor(s) and not of MDPI and/or the editor(s). MDPI and/or the editor(s) disclaim responsibility for any injury to people or property resulting from any ideas, methods, instructions or products referred to in the content.